ISSN 1062-8738, Bulletin of the Russian Academy of Sciences: Physics, 2023, Vol. 87, No. 11, pp. 1612–1617. © Pleiades Publishing, Ltd., 2023.
Russian Text © The Author(s), 2023, published in Izvestiya Rossiiskoi Akademii Nauk, Seriya Fizicheskaya, 2023, Vol. 87, No. 11, pp. 1580–1585.

Dielectric and Optical Properties of Gas Hydrates and Ices: Ab Initio Simulation Results

M. B. Yunusov[a, *] and R. M. Khusnutdinoff[a, b]

[a] *Kazan (Volga region) Federal University, Kazan, 420008 Russia*

[b] *Udmurt Federal Research Center, Ural Branch, Russian Academy of Sciences, Izhevsk, 426068 Russia*

**e-mail: mukhammadbek@mail.ru*

Received May 22, 2023; revised June 19, 2023; accepted July 28, 2023

Abstract—Dielectric tensors $\varepsilon_{ik}(\omega)$, optical absorption spectra $R(\omega)$, reflection spectra $a(\omega)$, and the density of electronic states $N(E)$ are calculated for the lattices of gas hydrates with sI and sH structures, and for ices I_h and I_{II}. The dependence of the dielectric permittivity on the type of guest molecules in the sI hydrate is discussed.

DOI: 10.3103/S1062873823703793

INTRODUCTION

Hydrates are complex crystal compounds in whose water lattices molecules of such low molecular weight gases as H_2, N_2, Ar, Kr, Xe, CO_2, H_2S, CH_4, and C_2H_6 are enclosed during nucleation [1]. Formed in the depths of natural zones with optimal thermobaric conditions (oceanic coastal zones, permafrost zones), hydrates normally form cubic sI and sII or hexagonal sH structures [2]. The sI hydrate (Fig. 1a) is the one most common in nature and is of the greatest interest for science and industry, since this type of hydrate is based on hydrocarbon gases important for the energy industry (methane, ethane) [3, 4]. The sI hydrate lattice has D- and T-type molecular cavities but no fixed order in the arrangement of protons. The D cavity is described by the geometric formula 5^{12} (formed by 12 pentagons), contains 20 H_2O molecules, and has characteristic diameter $d \approx 5$ Å. The T cavity is described by the geometric formula $5^{12}6^2$, contains 24 H_2O molecules, and has characteristic diameter $d \approx 6$ Å. The sH hydrate (Fig. 1b) forms around two types of hydrate forming gases, e.g., CH_4 and C_5H_{10}. Molecules with smaller radii fill the small D and D' cavities, while large molecules fill the large E cavities. The D' cavity is described by the geometric formula $4^35^66^3$, contains 20 H_2O molecules, and has a characteristic diameter $d \approx 5$ Å. The E cavity is described by the geometric formula $5^{12}6^8$, contains 36 H_2O molecules, and has characteristic diameter $d \approx 9$ Å. Hydrates belong to clathrate systems. These are crystals in whose lattices are vacant cavities that can include various molecules. The prospects for the use of clathrate systems, particularly hydrates, stimulate interest from science and industry. Hydrates are widely used in water filtration technologies and as gas storage tanks [5]. In addition, large reserves of methane in gas hydrate deposits in the bowels of the Earth, reaching 10^{18} m^3 according to some estimates, could become the main sources of hydrocarbon fuel [3]. The mechanical, thermal, optical, and electronic characteristics of gas hydrates and ices are almost identical. However, hydrates (in contrast to ices) are non-stoichiometric complex compounds that contain various gases in their crystal cavities.

Hexagonal ice I_h is the most common solid phase of water in nature. Water molecules in I_h ice line up in a hexagonal lattice similar to a honeycomb (Fig. 1c), oxygen atoms are located at the lattice nodes, and the edges are formed by hydrogen bonds between them. The location of hydrogen atoms in the crystal lattices of hydrates obeys the Bernal–Fowler ice rule [6]. I_h ice is a proton disordered structure, meaning there are many lattice configurations that are equal in potential energy and differ in the distribution of nuclei of hydrogen atoms. Each of these configurations obeys the Bernal–Fowler rule. Under high pressure, $p \in [0.2; 0.5]$ GPa, which is seen in the bowels of the Earth, hexagonal ice transitions to the I_{II} ice phase (Fig. 1d) [7]. I_{II} ice has proton ordering and a crystal structure in the form of parallel hexagonal channels that can contain guest molecules up to 3.5 Å in size (helium, hydrogen) [8], thereby exhibiting the properties of clathrate compounds.

Many experimental and theoretical works have been devoted to studying the thermophysical and mechanical properties, structural features, and processes of nucleation and dissociation of ices and gas hydrates [1–12]. Of great theoretical and practical importance is the study of the electronic properties [13, 14], dielectric tensors, and optical spectra [15–24]

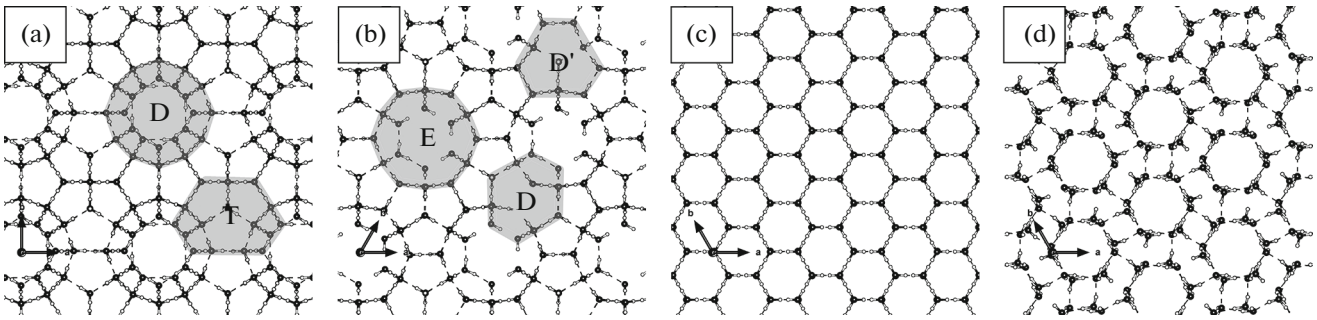

Fig. 1. Crystal lattices of (a) sI hydrate, (b) sH hydrate, (c) I_h ice, (d) I_{II} ice. Oxygen atoms are on the lattice nodes; edges are formed by hydrogen O–H bonds.

of the crystal lattices of ices and hydrates, which remain poorly studied due to technical limitations. Knowledge of the dielectric and optical properties of clathrate compounds will contribute to the improvement of electromagnetic means for the exploration and analysis of gas hydrate deposits. There is a controlled source electromagnetic survey (MCSEM) technique that can be used to obtain data on the electrical resistivity of rock formations up to 4 km deep and determine if there are gas hydrate deposits in it [16]. Time-domain reflectometry (TDR) is also used, with which we can obtain data on the volumetric dielectric characteristics of a sample and estimate the concentration of gas hydrate in it [17]. Information about the dielectric and optical characteristics of ice is therefore of practical importance and will allow us to distinguish potential gas hydrate deposits from an ice mass that does not contain gas.

SIMULATION DETAILS

Ab initio calculations were performed for ice lattices I_h and I_{II}, hydrate lattices sI and sH, and hydrate lattices sI with Xe, H_2S, CO_2, CH_4, C_2H_6 and C_3H_6 gases. The ways of filling the cavities with different gases was considered: small Xe, H_2S, CH_4 molecules can be included in small D and large T cavities, while CO_2, C_2H_6 and C_3H_6 molecules can only fill T cavities. The crystal lattices of the systems studied in this work are shown in Fig. 1.

The dielectric and optical characteristics were calculated via ab initio simulation using the density functional theory [25, 26]. This was done by transitioning from wave functions to electron density (1) and then solving the Kohn–Sham system of Eqs. (2) with allowance for effective one-electron self-consistent potential (3), which is the sum of the external potential, the Coulomb potential, and the derivative of the energy of exchange correlation:

$$n(r) = \sum_{i\sigma} |\varphi_{i\sigma}(r)|^2, \tag{1}$$

$$\left(-\frac{1}{2}\nabla^2 + V_{\text{eff}}(r)\right)\varphi_{i\sigma}(r) = \varepsilon_{i\sigma}\varphi_{i\sigma}(r), \tag{2}$$

$$V_{\text{eff}}(r) = V_{\text{ext}}(r) + V_{\text{H}}(r) + V_{\text{XC}}(r)$$
$$= V_{\text{ext}}(r) + \int \frac{n(r')\,dr'}{|r - r'|} + \frac{\delta E_{\text{XC}}[n(r)]}{\delta n(r)}. \tag{3}$$

Simulation was done with the specialized VASP package [27, 28], in which a pseudopotential approach is used to describe ion–electron interactions. The principle of pseudopotentials consists of replacing the rapidly oscillating wave functions of electrons near atomic nuclei with smoother functions, while preserving the norm of the wave function and the potential of the nuclei. This allows us to substantially optimize calculations. In this work, we used the pseudopotential PAW (projected plane wave) approach [29]. Exchange–correlation interaction was considered in the generalized gradient approximation (GGAPBE) [29, 30]. The system's energy was minimized using the RMM-DIIS algorithm [31]. Partitioning of the k-space by a 2 × 2 × 2 grid was used, and a convergence in energy of 10^{-4} eV was achieved. Periodic boundary conditions were imposed on the modeling cells.

The static dielectric tensor was calculated within the density functional perturbation theory using the LEPSILON= .TRUE. function in the VASP package. To calculate the frequency-dependent dielectric function, we used launched calculations in VASP using the LOPTICS= .TRUE. function. The ε(ω) tensor was calculated after reaching the ground state of the electron subsystem based on single-particle wave functions of electrons. The imaginary part of the tensor was determined by summing over all states using Eq. (4):

$$\varepsilon_2^{\alpha\beta}(\omega) = \frac{4\pi^2 e^2}{\Omega}\lim_{q\to 0}\frac{1}{q^2}\sum_{\text{v,c},k} 2W_k \delta(\varepsilon_{ck} - \varepsilon_{vk} - \omega)$$
$$\times \langle u_{ck+q\text{e}\alpha} | u_{vk}\rangle \langle u_{ck} | u_{vk+q\text{e}\beta}\rangle^*, \tag{4}$$

where index k is the number of k-points in the Brillouin zone, W_k is the weight of k-points, indices c and v refer to the electronic states of the conduction and

Table 1. Static dielectric tensors of ices and hydrates. Axes z are co-directed with the vectors from unit cells in Fig. 1

System	ε_{xx}	ε_{xy}	ε_{xz}	System	ε_{xx}	ε_{xy}	ε_{xz}
	ε_{yx}	ε_{yy}	ε_{yz}		ε_{yx}	ε_{yy}	ε_{yz}
	ε_{zx}	ε_{zy}	ε_{zz}		ε_{zx}	ε_{zy}	ε_{zz}
I_h	1.879	0.000	0.000	sI + H_2S	1.996	0.001	0.001
	0.000	1.879	0.000		0.001	1.971	0.000
	0.000	0.000	1.887		0.001	0.000	1.972
I_{II}	2.013	0.000	0.000	sI + CO_2	1.754	0.002	0.001
	0.000	2.013	0.000		0.002	1.752	0.001
	0.000	0.000	2.041		0.001	0.001	1.877
sH	1.610	–0.001	–0.001	sI + CH_4	1.855	0.001	0.001
	–0.001	1.608	–0.001		0.001	1.852	0.000
	–0.001	–0.001	1.620		0.001	0.000	1.852
sI	1.628	0.001	0.000	sI + C_2H_6	1.905	0.002	0.000
	0.001	1.625	0.000		0.002	1.903	0.001
	0.000	0.000	1.625		0.000	0.001	1.937
sI + Xe	2.005	0.001	0.001	sI + C_3H_6	2.010	0.002	0.001
	0.001	2.003	0.000		0.002	2.008	0.000
	0.001	0.000	2.003		0.001	0.000	1.964

valence bands, and u_{ck} is the periodic part of the orbital wave function at the k-point. The real part of the frequency-dependent dielectric tensor was calculated from the imaginary part using the Cramer–Kronig equation

$$\varepsilon_1^{\alpha\beta}(\omega) = 1 + \frac{2}{\pi}\int_0^\infty \frac{\varepsilon_2^{\alpha\beta}(\omega')\omega'}{\omega'^2 - \omega^2} d\omega'. \quad (5)$$

RESULTS AND DISCUSSION

Dielectric tensor $\varepsilon_{ik}(\omega)$ characterizes the propagation of electromagnetic radiation of different frequencies in dielectric volume (6). Tensor ε_{ik} of static permittivity is the limiting case ($\omega \to 0$) of tensor $\varepsilon_{ik}(\omega)$ and describes the field in a dielectric placed in a constant electric field:

$$D_i = \varepsilon_{ik}(\omega) E_k. \quad (6)$$

The static dielectric tensor ε_{ik} was calculated for each crystal system (Table 1). The crystal lattices of I_h ice and sH hydrate have hexagonal symmetry, while the crystal lattice of I_{II} ice has trigonal symmetry. Theoretically, the lattices of I_{II}, I_h and sH should be uniaxial systems in terms of the dielectric tensor and optical properties [32]. Results from calculating permittivity (Table 1) show that the I_h, I_{II}, and sH systems have axes ε_{zz}, which coincide with the unit cell vectors in Fig. 1. The crystal lattice of sI hydrate has cubic symmetry and should exhibit isotropy in terms of dielectric and optical properties; i.e., the diagonal components of the dielectric tensor should coincide ($\varepsilon_{zz} = \varepsilon_{xx} = \varepsilon_{yy}$), as was confirmed by calculations. Dielectric constant value $\varepsilon \approx 1.88$ for I_h ice; $\varepsilon \approx 2.01$ for I_{II} ice; $\varepsilon \approx 1.61$ for sH hydrate lattice; and $\varepsilon \approx 1.63$ for sI hydrate lattice. An increase in the values of the dielectric tensor components is observed when the sI hydrate lattice includes different gases. Average permittivity $\varepsilon \approx 2.00$ for the Xe hydrate; $\varepsilon \approx 1.98$ for the H_2S hydrate; $\varepsilon \approx 1.85$ for the CH_4 hydrate; $\varepsilon \approx 1.92$ for C_2H_6 hydrate; and $\varepsilon \approx 1.98$ for C_3H_6 hydrate, which is higher than the value for an unfilled sI framework ($\varepsilon \approx 1.63$). The dielectric constant therefore grows, due to the contribution from gas molecules to the polarizability of the hydrate crystals. Components ε_{zz}, ε_{xx}, ε_{yy} are close in magnitude for the sI hydrate with molecules whose symmetry is close to spherical (Xe, H_2S, CH_4, C_2H_6 and C_2H_6). The sI hydrate with a CO_2 molecule has a pronounced anisotropy along axis z ($\varepsilon_{zz} \approx 1.88$, $\varepsilon_{xx} \approx \varepsilon_{yy} \approx 1.75$). This is because the CO_2 molecule has an extended shape and, being in an ellipsoidal T cavity, occupies a fixed orientation with a minimal energy value. This effect was considered in [33]. The ordered arrangement of CO_2 molecules in the unit cell of the sI crystal results in anisotropy of the dielectric properties along the corresponding axis.

The frequency-dependent components of dielectric tensor $\varepsilon_{ik}(\omega)$ for the frameworks of sI, sH hydrates

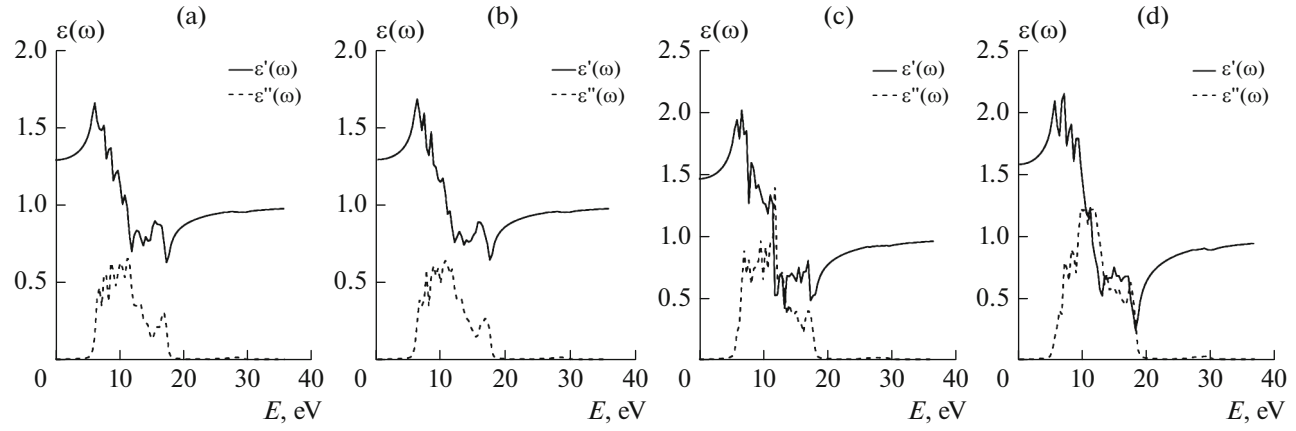

Fig. 2. Real ε'(ω) and imaginary ε"(ω) parts of the dielectric function for (a) sH hydrate, (b) sI hydrate, (c) I_h ice, and (d) I_{II} ice.

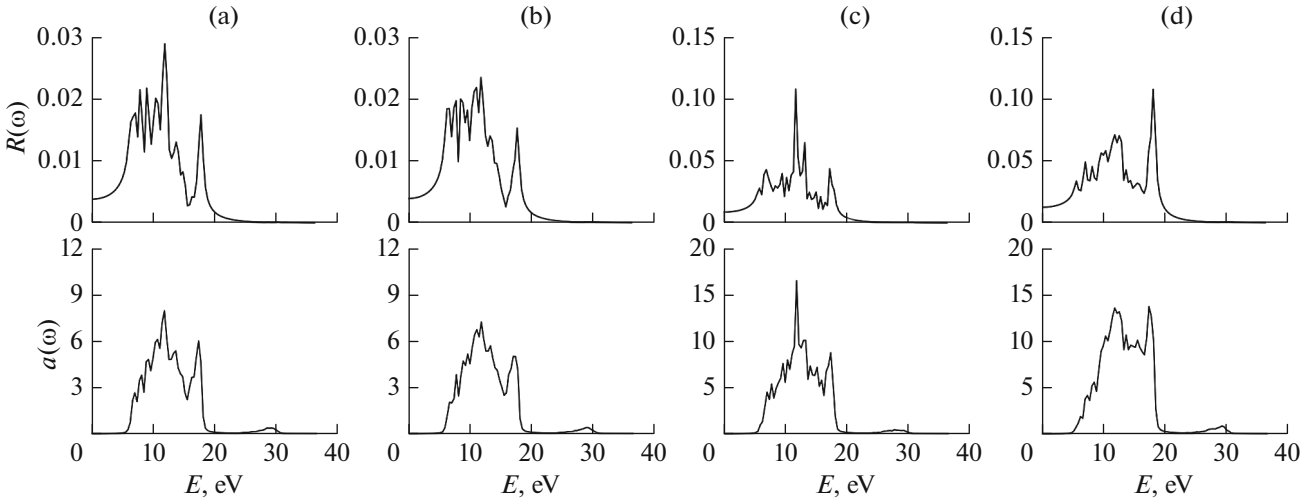

Fig. 3. Calculated spectra of reflection $R(\omega)$ and absorption a(ω) for (a) sH hydrate, (b) sI hydrate, (c) I_h ice, and (d) I_{II} ice.

and I_h, I_{II} ices were calculated with formula (7), averaged, and shown in Fig. 2.

$$\varepsilon_{ik}(\omega) = \varepsilon'_{ik}(\omega) + i\varepsilon''_{ik}(\omega). \quad (7)$$

The presented samples of ices and hydrates have a similar type of the dielectric function dependence on the external electromagnetic field frequency. Functions ε'(ω) and ε"(ω) allowed us to calculate many important optical characteristics of the medium (e.g., reflection $R(\omega)$, absorption $a(\omega)$, refractive indices $n(\omega)$ and $k(\omega)$) and loss function $L(\omega)$ [34]. In this work, we present only results from calculating reflection $R(\omega)$ and absorption $a(\omega)$ spectra using formulas (8) and (9) (Fig. 3). The formulas are given in a system of units where $c = 1$:

$$R(\omega) = \left|\frac{\sqrt{\varepsilon'(\omega) + i\varepsilon''(\omega)} - 1}{\sqrt{\varepsilon'(\omega) + i\varepsilon''(\omega)} + 1}\right|^2, \quad (8)$$

$$a(\omega) = \sqrt{2}\omega\left[\sqrt{\varepsilon'^2(\omega) + \varepsilon''^2(\omega)} - \varepsilon'(\omega)\right]^{1/2}. \quad (9)$$

Reflection spectra $R(\omega)$ show that the radiation reflected from I_h, I_{II} sI and sH latices was distributed in the $E \in [5, 20]$ eV range of photon energies (i.e., in the near ultraviolet region). Spectra $a(\omega)$ show that in terms of optical absorption, the considered crystals also exhibited activity in region $E \in [5, 20]$ eV. The main absorption peaks are at the level of 11.8 eV and correspond to the transitions of 2*p* electrons of water molecules in the hydrate lattice.

At the next stage of our work, we obtained the densities of electronic states $N(E)$ for the sI, sH, I_h, and I_{II} crystal structures. As can be seen in Fig. 4a, the electron density distribution for ices and unfilled hydrate lattices had similar forms and were characterized by nonzero electron density in the range of −19 to −17 eV, which corresponds to the *s*-electrons of oxygen, a nonzero electron density in the range −6.6–0 eV, which corresponds to the valence band (*s*-electrons of hydrogen and *p*-electrons of oxygen) and a weakly populated conduction band at levels of 5.4–12 eV. The band gap in hydrates and ices is ≈5.5 eV, which corresponds to pronounced dielectrics. The densities of electronic

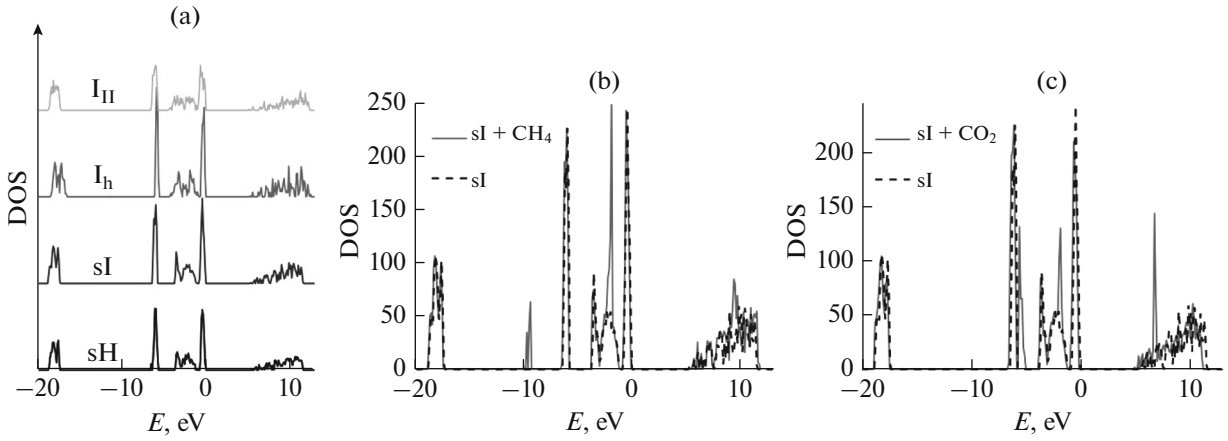

Fig. 4. Densities of electronic states (DOS) for (a) ices and lattices of hydrates, (b) sI hydrate with methane content, and (c) sI hydrate with CO_2 content.

states of the sI hydrate with a methane molecule inclusion in the D and T cavities and a carbon dioxide molecule in the T cavity are shown in Figs. 4b and 4c, respectively. These graphs contain an electron density peak at a level of 10 eV, associated with the presence of carbon atoms in the lattice cavities. A shift of the electron density toward lower energies was also observed when there was a guest molecule; this effect was especially noticeable when a carbon dioxide molecule was included. The drop in the energy of the electronic subsystem testifies to the stabilization of the clathrate framework by gas molecules.

CONCLUSIONS

Using a series of quantum mechanical calculations according to the density functional theory, we obtained static dielectric tensors ε_{ik} for I_h, I_{II} ices, unfilled lattices of sI, sH hydrates, and sI hydrates with naturally occurring hydrate formers (Xe, H_2S, CO_2, CH_4, C_2H_6 and C_3H_6). Complex frequency-dependent dielectric functions $\varepsilon(\omega)$ were calculated in the $E \in [0; 40]$ eV range of energies for I_h and I_{II} ices and sI and sH clathrate frameworks. Dielectric functions were used to calculate reflection $R(\omega)$ and absorption $a(\omega)$ spectra. The considered crystals were shown to exhibit optical activity in the region of $E \in [5, 20]$ eV in terms of absorption $a(\omega)$ and reflection $R(\omega)$. The main absorption peaks were at the level of 11.8 eV and corresponded to the transitions of $2p$ electrons of the framework's water molecules. Densities of electronic states $N(E)$ of an identical character were obtained for sI, sH, I_h, and I_{II} crystal structures and a band gap of ≈5.5 eV. Diagrams of the density of the electronic states of sI hydrate with methane molecules and inclusions of carbon dioxide show a slight shift of the electron density toward lower energies, testifying to the stabilization of the clathrate framework by gas molecules. The electronic, dielectric, and optical characteristics of sI, sH hydrates and I_h, I_{II} ices obtained in this work could be of both fundamental and practical importance by contributing to the development of electromagnetic ways of detecting and analyzing gas hydrate deposits.

ACKNOWLEDGMENTS

Our large-scale quantum mechanical calculations were performed on the computing cluster of Kazan (Volga Region) Federal University.

FUNDING

This work was supported by the Russian Science Foundation, project no. 22-22-00508.

CONFLICT OF INTEREST

The authors declare that they have no conflicts of interest.

REFERENCES

1. Sloan, E.D. and Koh, C.A., *Clathrate Hydrates of Natural Gases*, Boca Raton: CRC, 2007.
2. Takeuchi, F., Hiratsuka, M., Ohmura, R., et al., *J. Chem. Phys.*, 2013, vol. 138, no. 12, p. 124504.
3. Makogon, Y.F., *J. Nat. Gas Sci. Eng.*, 2010, no. 2, p. 45.
4. Kuznetsov, F.A., Istomin, V.A., and Rodionova, T.V., *Ross. Khim. Zh.*, 2003, vol. 47, no. 3, p. 5.
5. Su, F., Bray, C.L., Carter, B.O., et al., *Adv. Mater.*, 2009, vol. 21, no. 23, p. 2382.
6. Bernal, J.D. and Fowler, R.H., *J. Chem. Phys.*, 1933, vol. 1, no. 515, p. 420.
7. Fortes, A.D., Wood, I.G., Brodholt, J.P., and Vocadlo, L., *J. Chem. Phys.*, 2003, vol. 119, no. 8, p. 4567.
8. Zhdanov, R.K., Belosludov, V.R., Bozhko, Yu.Yu., et al., *JETP Lett.*, 2018, vol. 108, no. 12, p. 806.

9. Kirov, M.V., Manakov, A.Y., and Solodovnikov, S.F., *Bull. Russ. Acad. Sci.: Phys.*, 2009, vol. 73, p. 1535.
10. Shibkov, A.A., Kazakov, A.A., Verchenov, A.A., and Zolotov, A.E., *Bull. Russ. Acad. Sci.: Phys.*, 2007, vol. 71, no. 12, p. 1656.
11. van der Waals, J.H., *Trans. Faraday Soc.*, 1956, vol. 52, p. 184.
12. Monakov, A.Yu. and Dyadin, Yu.A., *Ross. Khim. Zh.*, 2003, vol. 47, no. 3, p. 28.
13. Yunusov, M.B., Khusnutdinoff, R.M., and Mokshin, A.V., *Phys. Solid State*, 2021, vol. 63, no. 2, p. 372.
14. Yunusov, M.B. and Khusnutdinoff, R.M., *J. Phys.: Conf. Ser.*, 2022, vol. 2270, no. 1, p. 012052.
15. Yunusov, M.B. and Khusnutdinov, R.M., *Fiz. Tverd. Tela*, 2023, vol. 65, no. 2, p. 328.
16. Jing, J.E., Chen, K., Deng, M., et al., *J. Asian Earth Sci.*, 2019, vol. 171, p. 201.
17. Wright, J.F., Nixon, F.M., and Dallimore, S.R., *Proc. 4th Int. Conf. on Gas Hydrates*, Yokohama, 2002, p. 1.
18. Wang, Z., Yang, L., Deng, R., et al., arXiv:1902.10914, 2019.
19. Kang, H., Jung, S., Koh, D.Y., et al., *Chem. Phys. Lett.*, 2013, vol. 587, p. 14.
20. Takeya, K., Zhang, C., Kawayama, I., et al., *Appl. Phys. Exp.*, 2009, vol. 2, no. 12, p. 122303.
21. Takeya, S. and Ripmeester, J.A., *Proc. 11th Int. Conf. on Gas Hydrates*, Edinburgh, 2011, p. 1.
22. Kobayashi, K., *J. Phys. Chem.*, 1983, vol. 87, no. 21, p. 4317.
23. Artemov, V.G., Volkov, A.A., and Sysoev, N.N., *Bull. Russ. Acad. Sci.: Phys.*, 2018, vol. 82, p. 59.
24. Volkov, A.A., Vasin, A.A., and Volkov, A.A., *Bull. Russ. Acad. Sci.: Phys.*, 2020, vol. 84, no. 9, p. 1053.
25. Hohenberg, P. and Kohn, W., *Phys. Rev.*, 1964, vol. 136, p. 864.
26. Kohn, W. and Sham, L.J., *Phys. Rev.*, 1965, vol. 140, p. A1133.
27. Kresse, G. and Furthmüller, J., *Phys. Rev. B*, 1996, vol. 54, no. 16, p. 11169.
28. Kresse, G. and Joubert, D., *Phys. Rev. B*, 1999, vol. 59, no. 3, p. 1758.
29. Perdew, J.P., in *Electronic Structures of Solids'91,* Berlin: Akademie, 1991.
30. Perdew, J.P., Burke, K., and Ernzerhof, M., *Phys. Rev. Lett.*, 1996, vol. 77, no. 18, p. 3865.
31. Pulay, P., *Chem. Phys. Lett.*, 1980, vol. 73, no. 2, p. 393.
32. Landau, L. and Lifshits, E.M., *Elektrodinamika sploshnykh sred* (Electrodynamics of Continuous Media), Moscow: Fizmatlit, 2005.
33. Yunusov, M.B. and Khusnutdinov, R.M., *Uch. Zap. Fiz. Fak. MGU*, 2022, no. 4, p. 2240702.
34. Sun, L., Zhao, X., Li, Y., et al., *J. Appl. Phys.*, 2010, vol. 108, no. 9, p. 093519.

Translated by E. Domoroshchina